# Degradation of alkali-activated slag subjected to water immersion

Liu, Chen; Liang, Xuhui; Chen, Yun; Li, Zhenming; Ye, Guang

**DOI**
10.1016/j.cemconcomp.2023.105157

**Publication date**
2023

**Document Version**
Final published version

**Published in**
Cement and Concrete Composites

Cement and Concrete Composites 142 (2023) 105157

Contents lists available at ScienceDirect

Cement and Concrete Composites

journal homepage: www.elsevier.com/locate/cemconcomp

# Degradation of alkali-activated slag subjected to water immersion

Chen Liu [a], Xuhui Liang [a], Yun Chen [a,b], Zhenming Li [a,c,*], Guang Ye [a,**]

[a] Department of Materials and Environment (Microlab), Faculty of Civil Engineering and Geoscience, Delft University of Technology, Delft, the Netherlands
[b] School of Materials Science and Engineering, South China University of Technology, Guangzhou, Guangdong, China
[c] Department of Materials Science and Engineering, The University of Sheffield, United Kingdom

ARTICLE INFO

*Keywords:*
Alkali-activated slag
Water immersion
Curing
Leaching
Carbonation

ABSTRACT

In this study, the impacts of tap water immersion on the pore solution, phase assemblages, gel chemistry and structure, and pore structure of alkali-activated slag (AAS) pastes were studied. AAS degrades under such condition and the potential mechanisms can be concluded as lower reaction rates, gel decomposition and carbonation. The leaching of $Na^+$ and $OH^-$ at early stages hinders the reaction of slag, which leads to a slower formation of reaction products. Long-term leaching can result in gel decomposition after 90 d. Coarsened gel pores and capillary pores are both identified in water-immersed samples. Additionally, the leached $Ca^{2+}$ can react with the dissolved $CO_2$ in tap water to form calcium carbonate. A calcium carbonate layer is observed surrounding the paste while the inner matrix is free of carbonation. The insights provided by this paper contribute to understanding the behaviors and durability of AAS in underwater conditions.

## 1. Introduction

Alkali-activated materials (AAMs) have gained significant academic and industrial interest in the last decades due to their promising potential as low-carbon binders compared to ordinary Portland cement [1–3]. Since AAMs have comparable or even superior properties to conventional Portland cementitious materials [4–6], AAMs have been increasingly implemented all over the world. Meanwhile, some manufacturing technology and quality assessments that are effectively used in the original Portland cement system are largely transplanted to AAM systems [1,2]. However, due to the distinction of chemistry involved in cement hydration and alkali activation, some techniques are not applicable in AAMs, such as the curing method. Curing primarily aims to maintain moisture in the cementitious materials by preventing the loss of water from the material during cement hydration. In general, water curing (including ponding, sprinkling and wet coverings) can be the most efficient compared to sealed and ambient curings, because water curing can provide further hydration of cement with external moisture and avoid drying problems [7–9]. However, in an AAM system, it is still controversial whether water curing is appropriate due to the existence of alkalis in pore solution and the consequent alkali loss [10–12].

Several studies have explored the influence of water curing on the properties of AAMs. Yao et al. [13] found that the water immersion could mitigate the linear shrinkage of alkali-activated slag-fly ash-based pastes, but undermined the compressive strength and pore structure. The XRD results showed that there was no evident difference in phase assemblage between the water-cured and sealed samples. It was assumed that the drop in compressive strength was caused by the excessive alkalis leaching from pastes. Huang et al. [11] examined the influence of different curing conditions (natural, sealed, fog and soak curings) on the compressive strength of alkali-activated bottom ash mortars. Fog curing led to the leaching of free cations and alkali ions, which significantly hindered the strength development. In addition, soak curing could further aggravate this adverse effect. Some studies proposed that intermittent water curing was the most effective curing regime for AAS concretes, where a reduction in porosity and sorptivity, and an increase in modulus of elasticity, and compressive strength were achieved [14,15]. Although there were some debates on the influence of water curing on the properties of AAMs, one consensus of the aforementioned literature was that leaching must occur when an AAM was in a humid or water condition.

Some works were carried out to investigate the impact of leaching on the property of AAMs. Zhu et al. [16] investigated the alkali leaching behavior and phase evolution of a 3-year-old alkali-activated-fly ash--slag-silica fume material. They found that about 30–40% of sodium in

* Corresponding author. Department of Materials Science and Engineering, The University of Sheffield, United Kingdom.
** Corresponding author.
*E-mail addresses:* zhenming.li@sheffield.ac.uk (Z. Li), G.Ye@tudelft.nl (G. Ye).

https://doi.org/10.1016/j.cemconcomp.2023.105157
Received 14 May 2022; Received in revised form 22 February 2023; Accepted 29 May 2023
Available online 30 May 2023

AAM subjected to water immersion could mobile freely and the alkali loss slightly coarsened the nano-sized pores in the binder. Besides, reaction products after 7 days of leaching were found to be stable and no notable pore coarsening or phase change was detected. Park et al. [17] studied the leaching behavior of alkali-activated slag and fly ash binders under an electrically accelerated condition. The paste containing more fly ash showed a higher extent of the dissolution of the binder. The C-A-S-H gel was more stable in comparison with the N-A-S-H gel, indicating that the stability of AAS in water was better than that of alkali-activated fly ash. Jia et al. [18] applied an in-situ observation technique to compare the leaching behavior of Portland cement (PC) and AAS pastes in $NH_4Cl$ solution (used for accelerating the dissolution of $Ca(OH)_2$ and C–S–H). Calcium in the gels of AAS paste was found more susceptible to leaching than that in PC due to the lack of portlandite with buffering capability in acid condition. In short, limited studies were conducted to understand the leaching issue of AAMs in an ambient water condition, and the previous works reported that AAMs after a short-term water immersion had no severe deterioration potential other than alkali leaching.

Despite many studies that have been done in terms of the leaching of AAMs, the degradation mechanism behind is still not clear. On one hand, there was a lack of theoretical statements to reveal how the alkali loss influenced the phase assemblages during the reaction of precursors and then how the phase assemblage led to a poor microstructure and consequently reduced properties of a water-immersed AAM. On the other hand, the stability of reaction products in long-term water immersion remained not completely understood. In addition, the previous works based on leaching mainly focused on slag-fly ash hybrid systems. Few studies could be found based on a sole slag-based system.

The purpose of this study, therefore, is to investigate the impact of external water on the property of AAS pastes and to clarify the mechanisms behind. To achieve this, AAS pastes derived from slag and NaOH or/and $Na_2SiO_3$ solutions are cured for 1 d and then cured in sealed and tap water conditions. The ion concentration of leachate and pore solution, reaction degree of slag, phase assemblages, gel chemistry, pore structure, and compressive strength of AAS pastes under these two conditions are compared. The degradation mechanisms of AAS paste due to water immersion are then discussed. The results are valuable for both curing regimes optimization and service life prediction in water conditions of AAS materials.

## 2. Materials and methods

### 2.1. Raw materials

The slag used in this work was supplied by ORCEM in the Netherlands. The chemical composition of slag, measured by a Panalytical Axios Max WD-XRF spectrometer, was shown in Table 1. A laser diffraction analyzer was used to test the particle size distribution of slag. The size of slag was in the range from 0.1 to 50 μm with a d 50 of 17.88 μm.

Sodium hydroxide (NaOH) pellets and water glass ($Na_2SiO_3$) were used for activator preparation. Per 100 g commercial water glass solution consisted of 8.25 g $Na_2O$, 27.5 g $SiO_2$, and 64.25 g water. The NaOH activator was prepared by dissolving NaOH pellets in deionized water, and the $Na_2SiO_3$ activator was prepared by mixing water glass, NaOH pellets, and deionized water. The activators were prepared one day before casting.

### 2.2. Mixture design

The mixture design is presented in Table 2. NaOH-based (NH) and $Na_2SiO_3$-based (NS) AAS pastes were synthesized at a constant $Na_2O$/slag ratio of 5% by mass. A Hobart mixer was employed for mixing. The activator was added to slag at low-speed mixing for 1 min and then another 1 min at high speed.

The outline of the experiments is presented in Fig. 1. The aim of this work is to simulate the most severe condition that an AAS paste can be suffered from. To this end, the samples used for micro-characterization were all sealed in a plastic tube for 1 day, then crushed into small pieces (2 mm–4 mm) before immersion to provide a fast-leaching condition. Mixtures for compressive strength were sealed and stored in a climate chamber at 20 °C. After 24 h, half of the hardened specimens were demoulded and then immersed in water, while others were continually cured in sealed condition. The samples were cured in a sealed or water immersion condition for up to 90 days. The distilled water was only used for tests regarding ion concentrations of leachate and pore solution (in section 2.3.1), inter alia, weekly refreshed tap water was applied for the other experiments.

### 2.3. Experimental methods

#### 2.3.1. ICP-OES

The ion concentration of the pore solution of hardened AAS samples was extracted by the steel-die method [19]. Pressure of up to 350 MPa was used to press the samples (about φ 25 mm × 40 mm, as shown in Fig. 1) cured in sealed and water-immersed conditions. The extracted pore solution was then filtered through Whatman 41 filter paper (20 μm) and the filtrate was diluted using nitric acid (0.2 vol %) for the measurement of Na, K, Ca, Al and Si by PerkinElmer Optima 5300DV ICP-OES spectrometer. The concentration of $OH^-$ was measured by titration against hydrochloride acid (0.1 mol/L) and phenolphthalein was used as the indicator. For the ion concentration of leachate, 10 g small piece samples (2–4 mm) were added into 100 g distilled water with a well-sealed plastic bottle as shown in Fig. 1. The bottles were shaken at a temperature of 20 °C. The leachate was collected after 7, 28, 60 and 90 days. The ion concentrations and the pH of the supernatant of the leachate were measured by ICP-OES instrument and titration, respectively.

#### 2.3.2. Selective dissolution

Basically, the degree of reaction of slag in a paste can be determined by the SEM image analysis and the selective dissolution test [20]. Given that a homogeneous material is required in the former method, the AAS samples after water immersion are not desirable to be measured in this way, as leaching is a depth-dependent problem and the degree of reaction of slag is thereby affected by this. As such, we employ a selective dissolution method to obtain a general reaction degree of slag in AAS pastes. The selective dissolution method for determining the reaction

**Table 2**
Mixture proportions of AAS pastes.

| AAS | Slag (g) | $SiO_2$ (mol) | $Na_2O$ (mol) | Water (g) | w/b | Ms |
|---|---|---|---|---|---|---|
| NH-based | 1000 | 0 | 0.8 | 430 | 0.43 | 0 |
| NS-based | 1000 | 0.8 | 0.8 | 430 | 0.43 | 1.0 |

w/b = water/binder ratio, Ms = $SiO_2/Na_2O$.

**Table 1**
Chemical composition of slag determined by XRF (%).

| | CaO | $Al_2O_3$ | $SiO_2$ | MgO | $Fe_2O_3$ | $SO_3$ | $K_2O$ | $TiO_2$ | other | LOI |
|---|---|---|---|---|---|---|---|---|---|---|
| Slag | 38.28 | 13.9 | 32.19 | 9.52 | 0.31 | 1.52 | 0.51 | 1.27 | 1.17 | 1.33 |

LOI: loss of ignition.

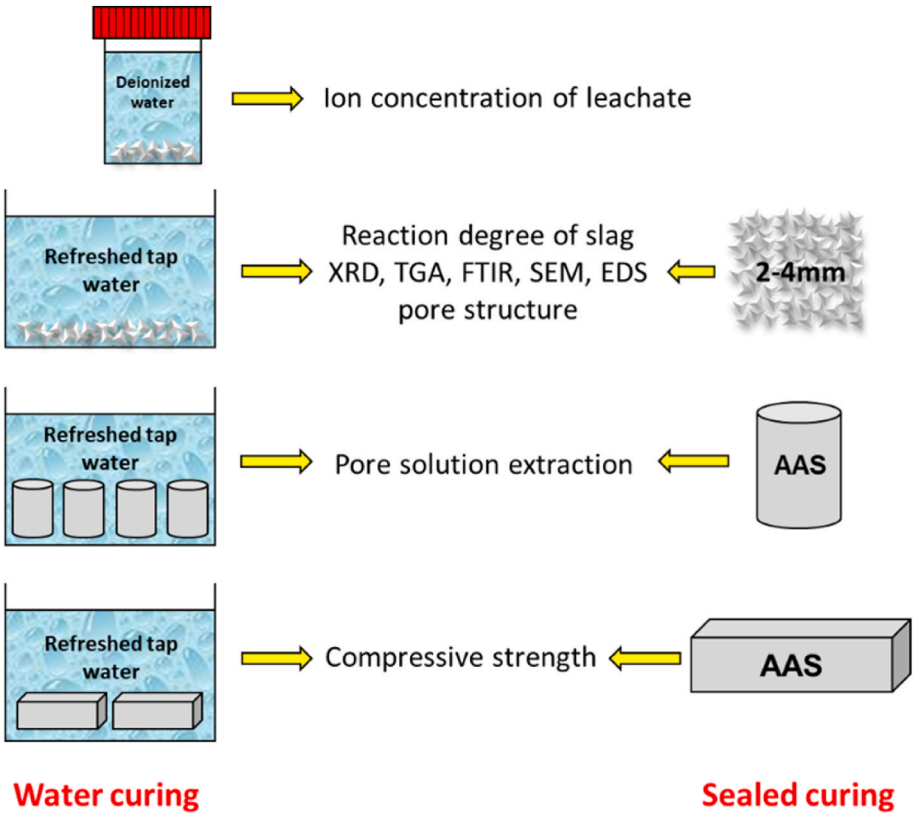


**Fig. 1.** Outline of the experiments. The characterization methods involved in this work include inductively coupled plasma-optical emission spectrometry (ICP-OES), X-ray diffraction (XRD) analysis, thermogravimetric analysis (TGA), Fourier-transform infrared spectroscopy (FTIR), scanning electron microscopic (SEM) and energy-dispersive X-ray spectroscopy (EDS).

degree of slag in cementitious materials has been implemented in previous studies [21–23]. Its principle was based on a preferential chemical extraction of the reaction products and unhydrated cement leaving the unreacted slag. A modified and widely-used method, so-called "salicylic acid-methanol" (SAM) extraction, was employed in this work [24]. The well-ground and hydration-arrested powder of samples (0.3 g) was added to a solution containing 30 mL methanol and 2 g salicylic acid. The sample was stirred for 1 h and followed by filtration. The insoluble residue was washed with deionized water and methanol several times until it reach a neutral pH. After that, the residue was dried at 105 °C until the mass was constant. At last, weighing the mass loss of the samples and calculating the reaction degrees of slag. It is noted that the calcium carbonate and hydrotalcite in the AAS cannot be dissolved by SAM method (see appendix in Fig. A1). The final reaction degree of slag was determined by TGA quantitatively. Four replicates were conducted for each mixture.

### 2.3.3. XRD, TGA, and FTIR

XRD and TGA were employed to identify the solid in the leachate as well as the phase assemblage of AAS in different curing conditions. FTIR was utilized to study the gel chemistry of AAS pastes. The fine powder samples are applied in these three measurements and the hydration stoppage of AAS pastes was via the solvent exchange method [25]. The piece samples were grounded in a mortar with isopropanol to avoid carbonation. After grounding for half an hour, the fine powder with isopropanol was stood for 15 min to have a full solvent exchange. Then, we filtered the samples with filter paper and a vacuum pump. During the filtering process, we used absolute alcohol to wash the samples several times and used diethyl ether at the last time washing for rapid drying. At this moment, the powder has almost dried in appearance. Finally, we collected the fine powder into a Petri dish and stored them in a drying oven at 40 °C for 10 min. After that, we stored the samples in a vacuum dryer before testing. After these pretreatments, all the free water can be removed from the sample and only the chemical-bound water would be left. XRD was performed using a Bruker D8 Advance diffractometer applying CuKα (1.54 Å) radiation. The hydration-arrested powder samples were scanned between 5° and 70°, with a step size of 0.02° and a dwell time of 5 s per step. TGA was conducted by NETZCH TG-449-F3-Jupiter. The powder samples were weighted and heated from 40 °C to 1000 °C with a heating rate of 10 °C/min in an argon atmosphere. FTIR was conducted using a Spectrum TM 100 Optical ATR-FTIR spectrometer with the wavelength of the spectrum ranging between 600 and 4000 $cm^{-1}$ with a resolution of 4 $cm^{-1}$.

### 2.3.4. SEM and EDS

SEM and EDS were performed to characterize the morphology and gel chemistry of AAS pastes. Morphology and elemental ratios of pastes and gels in different curing conditions were observed and determined by a Philips-XL30-ESEM microscope. The vacuum-dried samples were impregnated using a low-viscosity epoxy resin and then polished down to 0.25 μm. To enhance the conductivity of samples, carbon was used as raw material to coat the samples. The samples were tested under backscattering electron (BSE) mode at an acceleration voltage of 20 kV under a low vacuum. Point analysis of pastes was applied and 60 points were selected for each sample.

### 2.3.5. Pore structure characterization

Since the ultra-fine nanopores especially in the NS-based AAS pastes are beyond the detection limits of mercury intrusion porosimetry (MIP), the pore structure (from 0.3 to 300 nm) of the samples was measured by the nitrogen absorption (NA) test. The 2–4 mm hydration-arrested piece samples were used in this measurement. It was conducted on a Micrometrics Gemini VII 2390 V1.03 with a relative pressure ranging from 0.05 to 0.998.

#### 2.3.6. Compressive strength

The compressive strength of AAS pastes was tested with a loading speed of 2.4 kN/s, according to NEN-196-1 [26]. Six replicates were tested for one mixture to obtain an average value.

## 3. Results and discussion

### 3.1. Ions concentration

#### 3.1.1. Leachate

Fig. 1 shows the elemental concentration of leachate. Generally, the concentrations of all the detected ions increase with time, which is attributed to the gradient of ion concentration between the pore solution and leachate. The contents of most ions become steady until 60 d. In addition, the pH of the leachate of NH-based pastes is much higher than that of NS-based one, and the trends of Na, K and Al are consistent with pH as well. This may be due to a denser microstructure of NS-based paste. In a NS-based system, considerable soluble silicon ions like $[SiO(OH)_3]^-$ and $[SiO_2(OH)_2]^{2-}$ are already present and evenly distributed in the activator, viz. initial pore solution. The C–N-A-S-H gels can be formed immediately when Ca and/or Al are released from slag [27]. However, in a NH-based system, due to the lack of soluble Si in the activator, Si in the C–N-A-S-H gels can be provided by slag only. As a result, more gels can be formed in a NS-based paste compared with a NH-based one regardless of other factors, as reported intensively in Refs. [28,29]. On one hand, more gels need more Na to balance the charge of the interlayers of gels [30]. On the other hand, more gels benefit a denser microstructure (as shown in section 3.5), which can limit the migration of ions. Besides, due to the same dosage of $Na_2O$ in both of the activators, the initial pH of NH activator is much higher than NS activator. This is also a reason why the leachate of NH-based paste has a higher pH.

The concentration of Si in the leachate of NS group is higher than that in NH group, which is mainly attributed to the soluble silicate initially introduced by NS solution. However, compared with other ions, the concentrations of Si and Ca ions fluctuated within 90 days. Furthermore, their trends are almost the same. This phenomenon can be explained by the "dissolution-reprecipitation mechanism" proposed by Katrina et al. [31]. The increase of Si and Ca concentrations is due to the gradient of ion concentrations between the leachate and pore solution. The decrease of Si and Ca concentrations is probably attributable to Ca/Si reincorporation on the dissolving surface and the potential reaction products participated on the paste in an alkali condition. The "dissolution-reprecipitation" that occurs in the leachate is a kind of dynamic equilibrium process, which leads to the concentrations of Ca and Si fluctuating within a certain range. In brief, owing to the gradient of ion concentrations between internal AAS samples and external water, ions can simultaneously leach out with the extension of leaching time. Notably, it should be mentioned that the ion concentration in a real surrounding environment would be affected by the flowability of liquid/water and the frequency of exchanging water. Since the deionized water applied in this work was stagnant and not updated, more ions could leach out if the pastes are exposed to a flowing aqueous condition.

#### 3.1.2. Pore solution

Fig. 3 presents the elemental concentrations in the pore solution of AAS cured in sealed and water conditions. Regardless of the curing conditions, the pore solution composition is dominated by Na, while much lower concentrations of K, Si, Al and Ca are observed. Despite the tiny amount of K detected in slag as shown in XRF result (Table 1), K seems readily to leach out and is the only element whose concentration increases with time. This is because K is hard to be uptaken by the C-A-S-H gels in the Na-based activator system [32–34]. Moreover, the concentrations of Na and K in soaked pastes are only half of those in the sealed ones, and NH-based water-immersed pastes can show a larger reduction compared to sealed ones. This is because the looser pore structure of NH-based pastes (as shown in section 3.5) provides more and wider ion transportation paths for the ions.

The content of Al is much higher in NS than NH system, which agrees with the results found by Zuo et al. [35]. The concentration of Si in the pore solution of NS sealed paste is much higher than that in the NH sealed paste with the same dosage of $Na_2O$ due to the incorporation of soluble Si in the NS activator. Meanwhile, a significantly lower concentration of Si is identified in the NS water-immersed sample in contrast to the sealed one, indicating that large amounts of Si are free in the pore solution and can leach out at a very early age. In addition, the

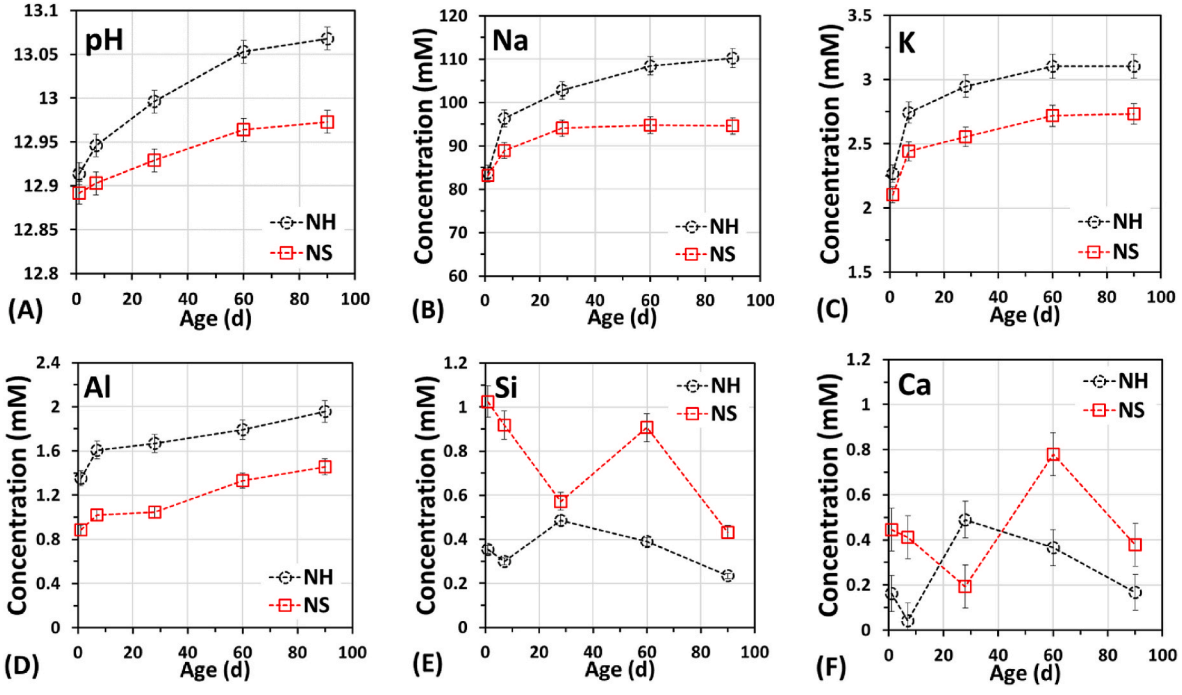


**Fig. 2.** pH and elemental concentrations of the leachate.

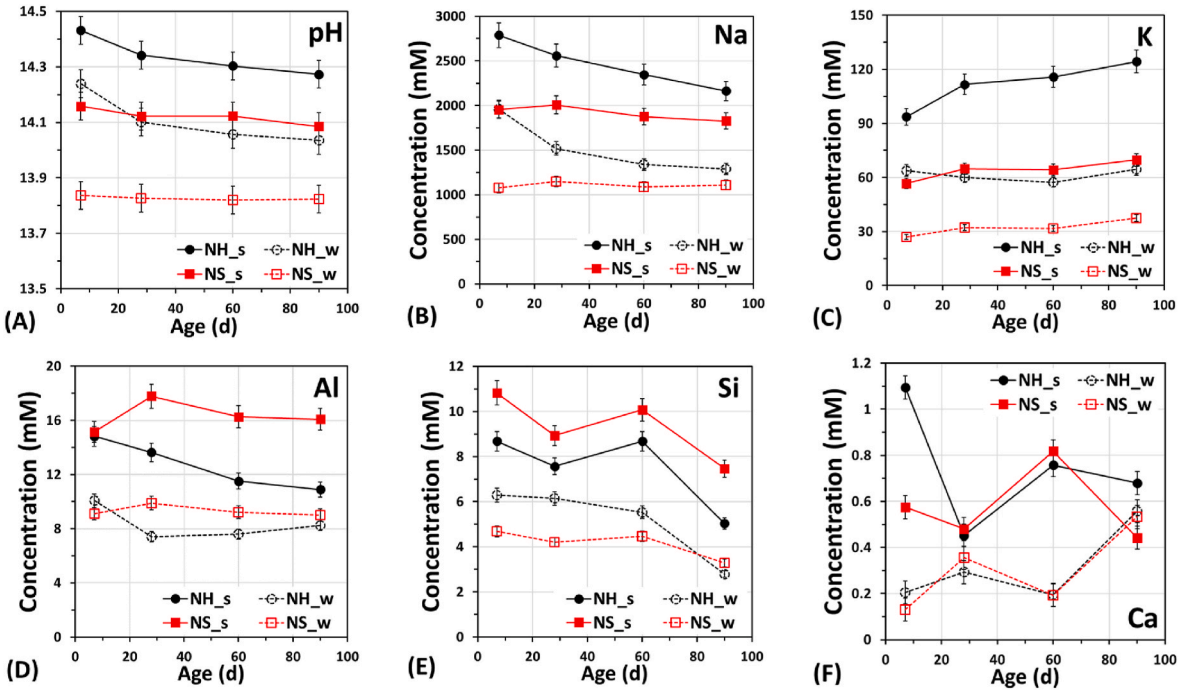


**Fig. 3.** Elemental concentrations and pH of the pore solution of AAS under sealed (s) and water immersion (w) conditions.

fluctuated trends of Ca and Si is again identified in both pastes which can be assigned to the dynamic equilibrium between the dissolution behavior of slag and the precipitation of gels to some extent [31,39]. Despite this, it is noted that the concentrations of all the detected elements (Mg is not measured since it is below the detected limit) in the pore solution of water-cured pastes, as well as the pH, are considerably lower than those in sealed pastes. Given the change of ion concentration due to leaching, the reaction environment of slag will change subsequently, which can influence the reaction degree of slag.

### 3.2. Reaction degree of slag

Fig. 4 shows the reaction degree of slag in AAS pastes cured in the sealed and water immersion conditions, respectively. In the sealed condition, the reaction degrees of slag in both pastes gradually increase with time and are over 50% up to 90 days. The reaction degree of slag in NH-based paste at 7 d is slightly higher than that of NS-based paste since a higher pH benefits the reaction of slag. However, the long-term reaction degree of slag in NH-based paste is lower, which is in agreement with [30]. This is because the initial fast gelation in a NH-based system leads to the formation of a dense layer covering the unreacted slag, which will slightly hinder the further reaction. Fortunately, the 90 d reaction degree of slag in the NH-based AAS is close to the NS-based one, suggesting that the so-called "rims" can not strongly influence the long-term reaction of slag.

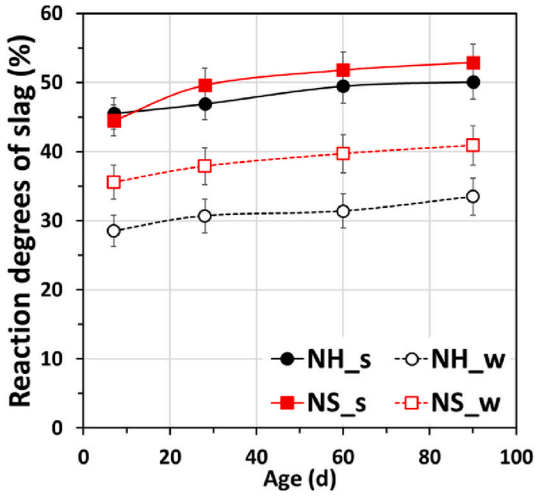


**Fig. 4.** Reaction degrees of slag of AAS pastes under sealed (s) and water immersion (w) conditions.

As shown in Fig. 4, the reaction degrees of slag in both two groups in water-cured condition are lower than that in sealed condition. As the leaching of ions and intrusion of water in the paste, the pH of pore solution becomes lower and lower with time (Fig. 3 (A)). Since a higher pH is beneficial for the disintegration of glassy phases in slag, AAS pastes cured in water have a lower reaction degree of slag. Notably, the gap between sealed and water-cured pastes in NH group is much larger than that in NS group, probably because a more porous microstructure of NH-based paste is more vulnerable to water ingress (as shown in section 3.5). Fortunately, although the piece AAS samples are immersed in water after 1 d, the chemical reaction of slag still maintains but with a relatively low rate.

### 3.3. Phase assemblage

#### 3.3.1. XRD analysis

At the earliest hours of water immersion, some flocculent solids were found on the bottom of the container with AAS samples. Fig. 5 shows the morphology and XRD pattern of the precipitated solids. The XRD result shows that the solid is actually calcium carbonate. Due to the leaching of alkali ions, the pH of the leachate increases gradually and the leachate can be considered an alkaline solution. Given the employment of tap water in this leaching test, the $CO_2$ dissolved in the leachate will spontaneously hydrolyze to bicarbonate ions ($HCO_3^-$) or carbonate ions ($CO_3^{2-}$) via a multi-step reaction sequence ($CO_2 + 2OH^- \rightarrow HCO_3^- + OH^- \rightarrow CO_3^{2-} + H_2O$) [37,38]. Afterward, carbonate ions will react with leached Ca ions from AAS pastes to precipitate calcium carbonate in the leachate. Note that the carbonation process here is different from what has been usually used to describe the reaction of paste/concrete with the $CO_2$ in the air.

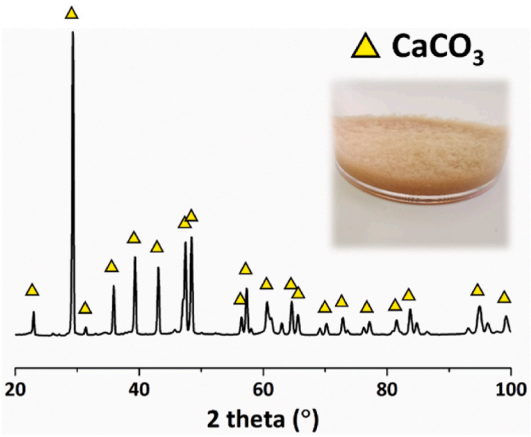


**Fig. 5.** Morphology and XRD of flocculent solid in the leachate.

Fig. 6 shows the XRD patterns of AAS pastes in different curing conditions. It is observed that calcium carbonate is present only in a water-immersed AAS paste and the density of which increases with leaching time. This is because the surface of piece samples is rough, which can provide considerable nucleation sites for the growth of calcium carbonates [39]. A calcium carbonate layer is identified in Fig. 11. According to the literature [40], 100 g of pastes are capable of bounding around 40–50 g of $CO_2$ in a Portland cement system. $Ca(OH)_2$ is a significant hydrate that can largely prevent the gels from being carbonated because it can decompose to calcium carbonate when exposed to $CO_2$ [41]. Nevertheless, due to the lack of $Ca(OH)_2$ in an AAS system, the intruded $CO_2$ will first react with Ca ions in the pore solution and subsequently the gels [42]. The reaction between $CO_2$ and gels will give rise to gel decalcification and even gel decomposition [43]. Therefore, the carbonation of AAS materials due to dissolved $CO_2$ in water should be noticed.

The intensity of the characteristic peaks of gels and hydrotalcite in both NH and NS-based sealed pastes increases with time. Furthermore, as a result of the more crystalized reaction products formed in NH system, the characteristic peaks of reaction products are more evident in NH-based pastes [30,44]. In the water-immersed AAS pastes, the signal of gels and hydrotalcite is substantially weaker in contrast to the sealed pastes at the same ages. On one hand, since a lower reaction degree of slag in water-cured AAS pastes, less amount of reaction products will be formed. On the other hand, as mentioned in section 3.1.2 (Fig. 3), the alkali loss and water ingress have significantly changed the alkaline environment of reaction products. The existing products are not stable and can be decomposed as an extension of time. Further evidence of the decomposition of reaction products is provided in the next section.

### 3.3.2. TGA

Fig. 7 shows the TG and DTG curves of AAS pastes under different curing conditions. According to Refs. [30,45–47], the reaction products in AAS systems can be distinguished by the weight loss among different ranges of temperatures: C–N-A-S-H gels (40–200 °C), hydrotalcite-like phases (200 and 400 °C) and calcium carbonate (600–800 °C) as shown in Fig. 8. In addition, the content of bound water obtained by measuring the weight loss up to 650 °C can be used as an indication of the total reaction products [48].

Generally, the gels, hydrotalcite and total bound water in sealed AAS pastes are significantly higher than that of water-immersed ones, which indicates that the content of reaction products is higher in sealed pastes. Notably, the gels, hydrotalcite and total bound water in sealed pastes constantly increase from 7 d to 90 d while that in water-immersed pastes first increase (from 7d to 60d) and then decrease at 90 d as shown in Fig. 8 (A)(B)(C). This evident drop is a reflection of the decomposition of reaction products. The alkali leaching leads to a decreased pH of the pore solution (Fig. 3), which could break the dynamic equilibrium between gels and pore solution. The ions that are initially uptaken by gels incline to escape from the structure due to the osmotic pressure caused by concentration gradients [49]. As the deceleration of gel formation at the later stage (Fig. 4), the gel decomposition becomes more dominant, which eventually leads to a decrease of bound water of gels at 90 d. In addition to gels, a slight reduction of hydrotalcite is identified in both two water-immersed AAS pastes as well. Such a decrease in hydrotalcite could be tentatively owing to carbonation [43]. Moreover, as shown in Fig. 8 (D), the amount of calcium carbonate monotonically increases with time. This is ascribed that the constant leaching can provide Ca ions that will subsequently react with aqueous $CO_3^{2-}$ to the formation of calcium carbonate on the surface of the paste.

## 3.4. Gel chemistry

### 3.4.1. FTIR

The FTIR spectra of all the AAS pastes are presented in Fig. 9. According to the literature [50,51], the main bands centered at around 940-970 $cm^{-1}$ represent the asymmetrical stretching vibration of Si–O-T (T = Si, Al) and/or Si–O-M (M = alkali metal elements), which is the characteristic structure of $Q^2$ units. The small shoulder around 1050 $cm^{-1}$ is assigned to the asymmetrical stretching of Si–O-T (T = Si or Al) bonds and/or Si–O-M bonds as well, but with a lower substitution of Al [52]. Another representative band of Si–O–Al or Si–O–Si regarding deformation vibration locates at around 900 $cm^{-1}$. The bands at 800-825 $cm^{-1}$ represent the Si–O stretching vibrations of the $Q^1$ unit [53].

As shown in Fig. 9 (A) and **(B)**, the signals of $Q^1$ and $Q^2$ in sealed AAS pastes are visible while their intensity and location have no obvious variation with time in both NH and NS pastes. The intensity of $Q^2$ in NH-based sealed paste is slightly stronger than that in NS-based one and the

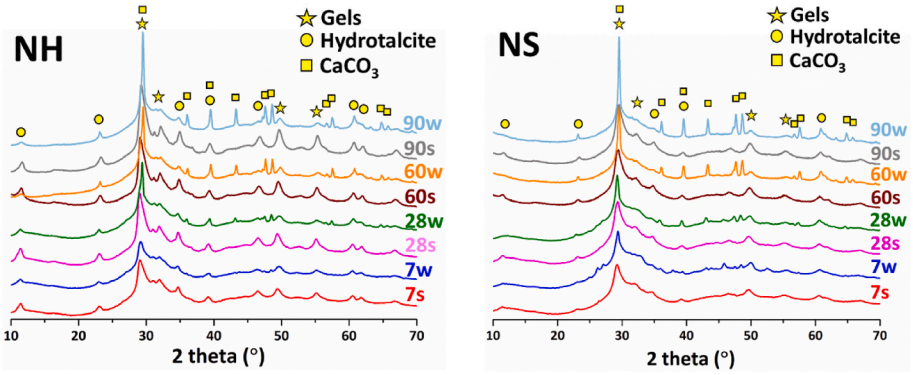


**Fig. 6.** XRD patterns of AAS pastes in sealed (s) and water immersion (w) conditions.

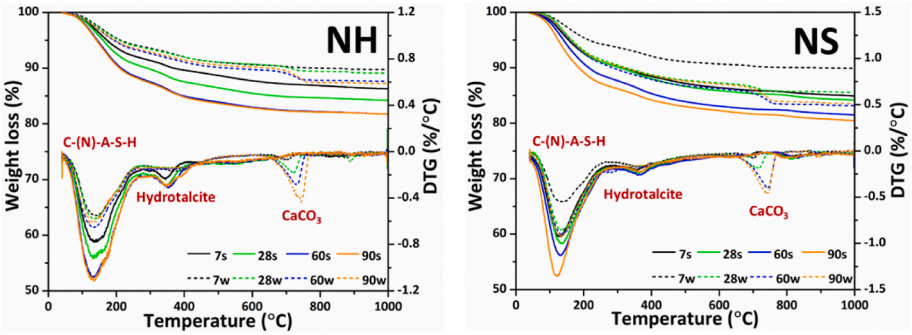


**Fig. 7.** TG and DTG of AAS pastes under sealed (s) and water immersion (w) conditions.

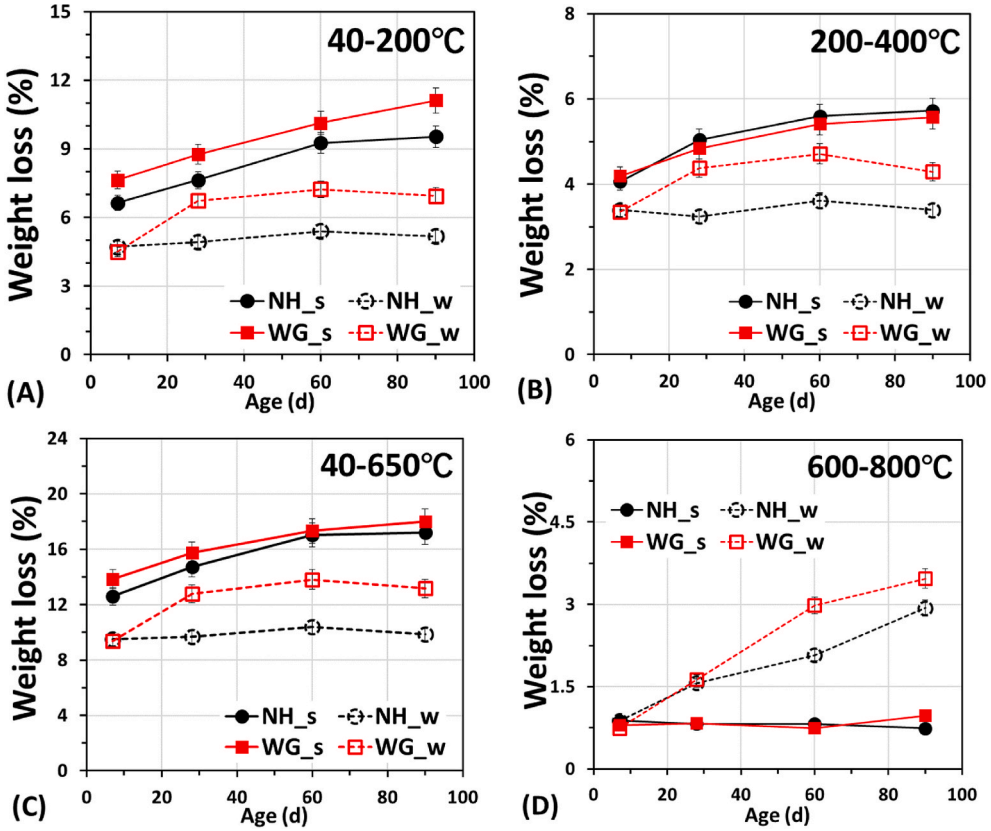


**Fig. 8.** Weight loss of AAS pastes normalized by mass at different temperature ranges in sealed (s) and water immersion (w) conditions. The weight losses between 40 and 200 °C, 200–400 °C, 40–650 °C and 600–800 °C can reflect the content of gels, hydrotalcite, total bound water of reaction products and calcium carbonate, respectively [30,45–48].

peak around 894 $cm^{-1}$ of NH-based sealed pastes is more evident than that of water-cured ones. This is an indicator that the bond of Si–O–Si and/or Si–O–Al in AAS pastes decreases after water immersion. Furthermore, since a large amount of soluble Si ions introduced by NS activator lead to a high concentration of Si in the pore solution (Fig. 3 (E)), C–N-A-S-H gels in NS-based paste will have a lower Ca/Si ratio (see section 3.4.2) than that of NH-based paste. As reported in Ref. [54], the content of $Q^1$ unit is increased with the increment of Ca/Si ratio. Hence, the NH-based AAS gets a higher intensity of $Q^1$.

The peaks regarding the bending ($v^2$) of $CO_3^{2-}$ [55] at around 875 $cm^{-1}$ are also detected in the water-immersed samples due to the presence of calcium carbonate. In addition, it is observed that the intensity of $Q^1$ and $Q^2$ units in water-immersed pastes is considerably weaker than that in sealed pastes. To better distinguish the differences in gels between sealed and water-immersed conditions, the bands at 930-970 $cm^{-1}$ ($Q^2$ unit) are amplified, as shown in Fig. 9(C) and (D). Generally, both the width and wavenumber of the $Q^2$ characteristic peak of NS-based sealed AAS are larger than that of NH-based sealed AAS. This is because the NS-based paste has a lower crystalized but higher cross-linked gel structure. As reported in Refs. [56,57], the width of the peak is dependent on the crystalization degree of gels (the sharper the peak, the higher the crystalization degree of the gel), while the wavenumber is assigned to the polymerization degree of gels (the higher the wavenumber is, the higher polymerization degree the structure obtains). Despite that FTIR results show little discrepancy among sealed AAS pastes at different ages, the wavenumbers regarding $Q^2$ in water-immersed samples are significantly higher than that in sealed condition regardless of curing ages. As reported in Refs. [53,54], the wavenumber of the peak (930–970 $cm^{-1}$) moves to a higher one as a decreased incorporation of Ca in C–N-A-S-H gels. Two possible reasons are available to explain this result. First, according to previous work [58], the Ca/Si ratio of C–S–H gels is decreased as an extension of

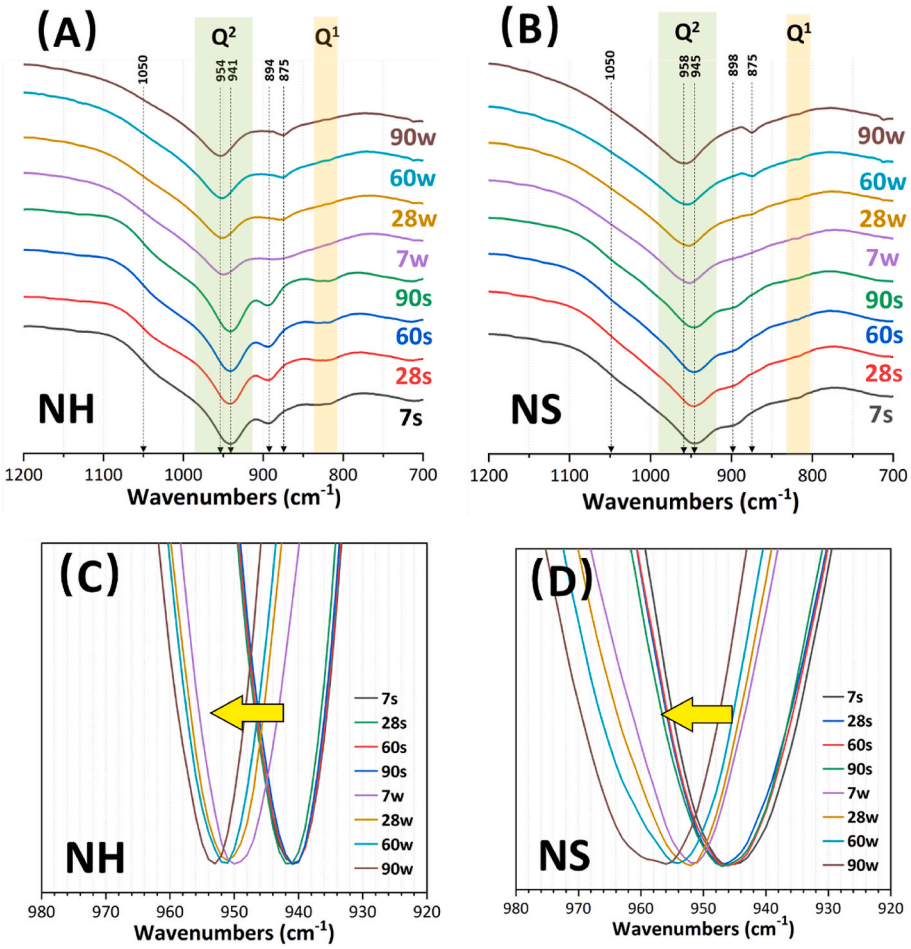


**Fig. 9.** FTIR spectra of AAS pastes under sealed (s) and water-immersed (w) conditions.

soaking time in the portland cement system. Second, intensive works claim that gel decalcification is a predominant feature when an AAS paste is carbonated [41,59,60]. Therefore, the constantly increased wavenumbers of $Q^2$ units are attributed to gels decalcification caused by immersion and carbonation.

### 3.4.2. SEM and EDS

Fig. 10 shows the morphology of NS-based AAS pastes at 28 d under different curing conditions. It is shown that the surface of a sealed piece of paste is smooth (Fig. 10 (A)) and the unreacted slag particles are closely surrounded by gels. In contrast, the surface of a water-immersed paste is rough (Fig. 10 (B)), which is covered by solid particles. The solid is actually calcium carbonate identified by EDS (as shown in Fig. 11), and the size of which ranges from nanoscales to microscales.

The cross-section of the surface part of the NS-based paste in sealed and water-immersed conditions is shown in Fig. 11. The most evident distinction between the two pastes is that there is a visible outer layer covering the internal matrix in the water-immersed paste. The bonding between the outer layer and matrix is not strong, and large cracks are formed near the dividing line. Based on the EDS results (see appendix Fig. A2 and Table A1), the outer layer is determined as calcium carbonate. Meanwhile, the result shows that calcium carbonate can be only detected at the outer layer, and intermixed reaction products of gel and calcium carbonate are rarely found in the inner part of the paste. This means that carbonation due to CO2 dissolved in water only occurs on the surface of AAS pastes, which is significantly distinct from the carbonation of pastes in the air or accelerated carbonation condition [41,42,60,61].

Fig. 12 shows the atomic Na/Si ratio verse Ca/Si ratio of AAS pastes measured by EDS. The internal part of a well-polished AAS sample was

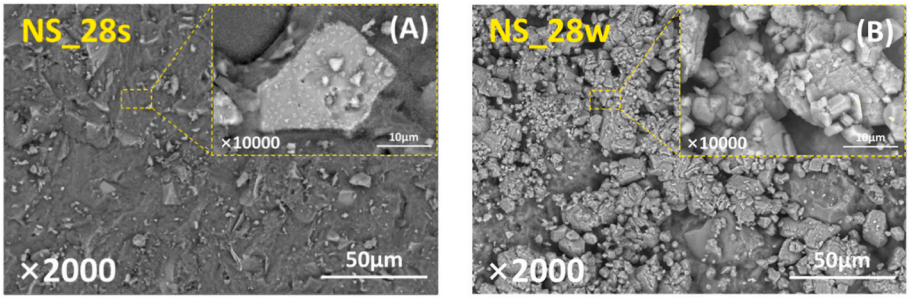


**Fig. 10.** Morphology of the surface of NS-based AAS pastes under sealed (s) and water immersion (w) conditions.

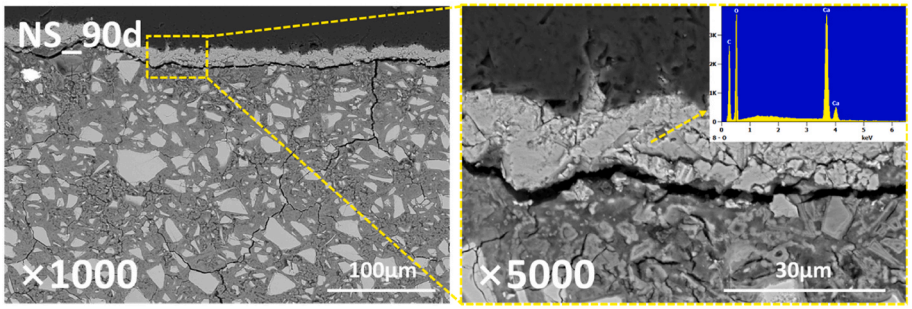


**Fig. 11.** Cross-section of the surface of the NS-based AAS paste after 90 d water immersion.

chosen for point analysis and 60 points were analyzed in each sample. As a large amount of soluble Si ions are in the initial NS activator, the Ca/Si ratio of NS-based sealed paste is generally lower than that of NH-based sealed paste. It is noticed that the Na/Si ratio of NS-based sealed paste significantly decreases from 7 d to 90 d whereas little variation of Na/Si is found in NH-based sealed paste between 7 d and 90 d. In the NS system, due to a large amount of soluble Si ions in pore solution, considerable gels can be formed in the system at 7 d but Na ions contribute more to balancing the charge between the interlayers of C–N-A-S-H gels at early ages due to the lack of Ca ions. With the extension of time, Ca ions are continually dissolved from slag and Na is gradually substituted by Ca in C–N-A-S-H gels [62]. In the NH system, as no soluble Si ions are available in the alkaline solution initially, Si ions can only stem from slag. Since the dissolution of Ca from slag is much easier than Si, Ca ions are always abundant when forming the C–N-A-S-H gels. Therefore, the Ca/Si ratio in NH-based AAS paste is relatively steady from 7 d to 90 d.

It is necessary to emphasize that the Na/Si ratio of AAS pastes after 90-day water immersion is almost zero in both two groups, which means Na can completely leach out at long-term water immersion. The desodiumization of gels verifies the hypothesis proposed by previous work [63]. Similarly, the slight drop in Ca/Si ratio is also identified as the extension of water-immersion time. This result is consistent with the decalcification of C–N-A-S-H gels found in FTIR (Fig. 9) and again indicates that Ca ions in gels are unstable after long-term leaching.

Fig. 13 shows the positive linear correlation between the Mg/Si and Al/Si ratios in AAS paste. As described by previous work [30,64–66], a linear correlation of Mg/Si with Al/Si suggests the existence of hydrotalcite-like phases, while the positive X-axis intercept presents the level of incorporation of Al in the C–S–H gels. The result shows that the

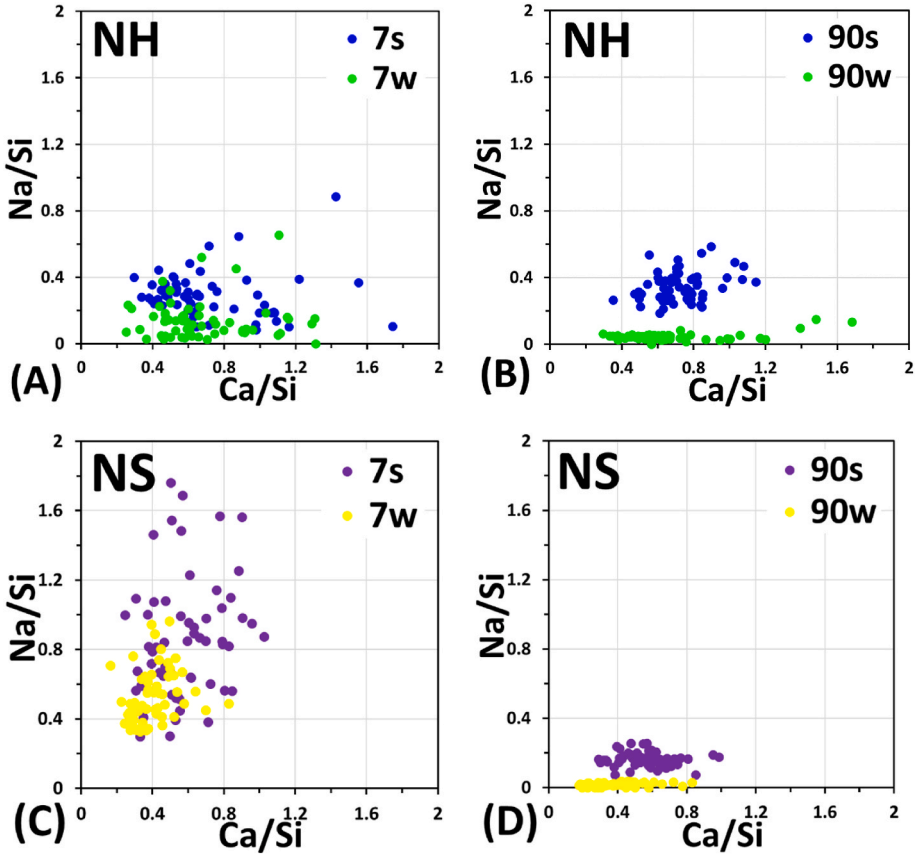


**Fig. 12.** Atomic Na/Si ratio versus Ca/Si ratio of AAS pastes under sealed (s) and water immersion (w) conditions.

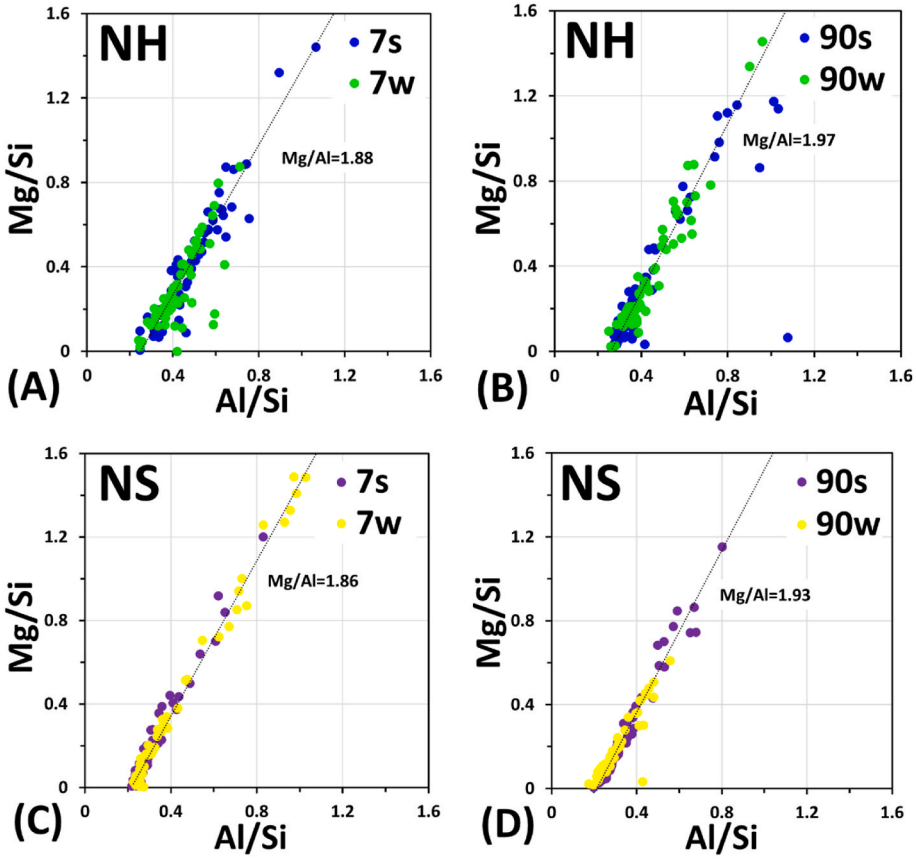


**Fig. 13.** Atomic Mg/Si ratio versus Al/Si ratio of AAS pastes in sealed (s) and water immersion (w) conditions.

average Al/Si ratio of gels in NH-based paste (about 0.24, Fig. 13 (A) and **(B)**) is slightly higher than that of NS-based paste (about 0.20, Fig. 13 (C) and **(D)**), which is in agreement with other work [65]. However, no evident difference in Al/Si ratio is identified between sealed and water-immersed pastes. This is probably because Si and Al are the structural elements of the gels, and both of them are hard to dissolve before the gel decomposes. In addition, the slopes of the trendlines, referring to the Mg/Al ratio, are well within the range from 1.92 to 4.35 representing hydrotalcite formed in an AAS paste [67,68]. The first aspect is that the Mg/Al ratio of the two pastes increases with time, and Mg/Al ratio is slightly higher in NH-based paste than the NS-based one. The second aspect is that the trendlines of Mg/Al ratio in sealed and water-immersed pastes overlap considerably, which suggests that the elemental component of hydrotalcite is steady after leaching. By the way, the drop of hydrotalcite in water-immersed AAS pastes from 60 d to 90 d determined by TGA (Fig. 8 (B)) can be also attributed to the same proportion of dissolution of hydrotalcite.

### 3.5. Pore structure

Given the employment of 1 d samples for water immersion, the water cannot migrate too much into the matrix, since the initial piece pastes have relatively high water content. Due to the gradient of ion concentration between the external water and pore solution, ion exchange can happen via the communicated capillary pores in the matrix. Therefore, the tortuosity and volume of the pore structure are expected to be understood. Fig. 14 (A) and **(B)** show the pore volume and pore size distribution of NH-based AAS pastes, respectively. As reported in Ref. [69], the pore ranging from 0 to 100 nm in an AAS paste can be classified as gel pores (0–10 nm) and capillary pores (10–100 nm). The pore volume of NH-based pastes (Fig. 14 (A)) in sealed condition is decreased as a function of time while that of water-immersed pastes is increased with time generally. Due to the limited detecting range (1 nm–300nm) of pore structure by NA test, the volume of pores larger than 300 nm in NH-based pastes is not included. The reason why the water-immersed paste at 90 d has low pore volume than that at 60 d is probably that 90-day-immersed paste has a high volume of big capillary pores which is beyond the measurement range. Anyhow, as shown in the pore distribution (Fig. 14 (B)), both the gel pore and capillary pore in the water-immersed paste are increased with time. The pore structure of NH-based AAS is significantly coarsened after water immersion.

Fig. 14 (C) shows the pore volume of NS-based AAS pastes. Similarly, almost zero pore volume is detected in the sample that is sealed curing for 90 d, and the pore volume of the water-immersed paste is much higher than that of the sealed one. However, compared with NH-based pastes, NS-based AAS is likely to show less influence, as the pore structure of the water-immersed sample can still be densified within 60 days, which is in agreement with the result of gel content in Fig. 8. Furthermore, the pore volume of water-immersed paste at 90 d is even higher than that at 7 d. The degradation of microstructure is owing to the decomposition of reaction products in long-term water immersion, as interpreted in section 3.3.

Fig. 14 (D) shows the pore size distribution of NS-based AAS pastes. Water-immersed pastes show higher content of gel pores compared with sealed pastes. Similar results can be found in others' work as well [13,16]. Since the content of gels formed in a water-immersed paste is less than a sealed one as shown in the above sections, the packing of gels will be much looser in water-immersed condition and thus more nano-sized pores are detected. The gel decomposition in NS-based paste is well reflected by the increment of gel pores at 90 d, which is in agreement with the trend of gel content as shown in Fig. 8. In addition, gel decomposition will also cause the increment of capillary pores. As

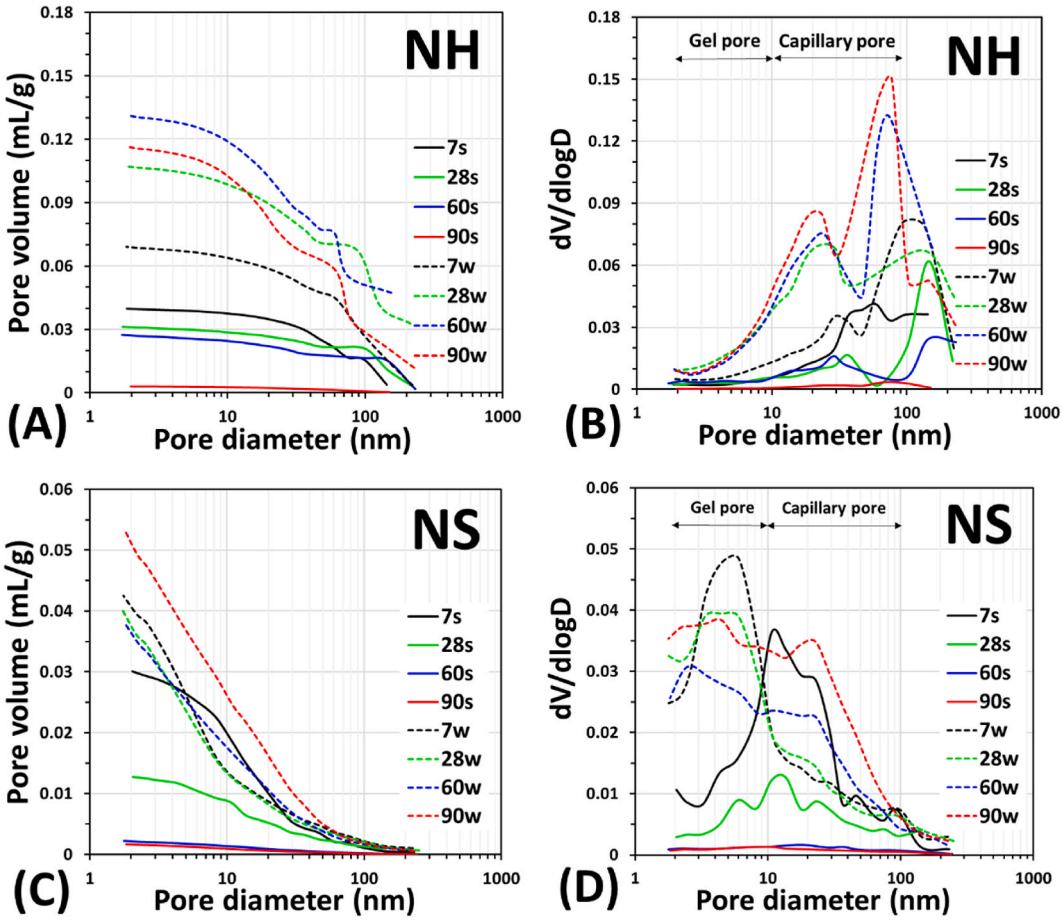


**Fig. 14.** Pore volume and pore size distribution of AAS pastes under sealed (s) and water immersion (w) conditions.

shown in Fig. 14 (D), the 10 nm–100 nm capillary pores are considerably increased with time, especially at 60 d and 90 d.

### 3.6. Compressive strength

Fig. 15 shows the compressive strength of AAS pastes as a function of time. The compressive strength of NS-based pastes is higher than that of NH-based pastes, which is assigned to a finer pore structure of NS-based AAS pastes. In addition, the compressive strength of water-immersed pastes is lower than sealed pastes at the same ages. More specifically, the compressive strength of NH and NS-based water-immersed pastes are lower than sealed pastes by 15% and 12%, respectively. Therefore, it can be concluded that water-immersed condition is detrimental to the compressive strength of an AAS paste. Admittedly, it should be mentioned that a higher moisture content in the sample itself can mean a lower compressive strength due to the effects of higher capillary pressure or lower interparticle bonds [Ref added: Neville, A.M. and Brooks, J.J., Concrete Technology, Pearson Education Limited, 2010]. It is not clear yet how much reduction was contributed by difference in curing condition and how much was caused by different moisture contents.

In addition, it is worth noting that the deviations of compressive strength of water-immersed paste are much larger than sealed one, especially for NS-based pastes. A similar result is also found in Ref. [13]. This phenomenon is attributable to the gradient of stress formed in the samples [70]. a NS-based AAS paste is commonly subjected to the shrinkage problem and cracking potential due to the self-desiccation [71–74]. To fully relieve this stress, ingressed water is expected to diffuse from the surface to the interior at a certain rate to compensate the autogenous shrinkage. This process is highly dependent on the permeability and size of the sample. A dense microstructure of NS-based paste gives rise to the insufficiently rapid migration of water from outside to inside. Thus, a stress gradient developed. The sample in such a state is inclined to have more likelihood of cracking potential than the homogeneous stress distribution of the sample in sealed condition. Therefore, NS-based water-immersed pastes have much larger deviations and even the retraction of compressive strength at 90d.

## 4. Summary and perspective

Based on the above results, the outcomes of an immature AAS paste in the water-immersed condition can be summarized in Fig. 16, in which three main degradation mechanisms can be abstracted.

### 4.1. Low reaction rate

When an immature hardened AAS paste (e.g. cured for 1 day in this work) is immersed into water, large amounts of alkali ions ($Na^+$, $K^+$, $Ca^{2+}$) and hydroxide ions are liable to leach out (Fig. 2). The concentrations of different ions in the leachate generally increase with time due to the gradient of ion concentrations. Meanwhile, the ion concentration as well as pH of the pore solution is decreased as a function of water-immersed time, which is significantly lower than that in a sealed AAS paste at the same ages (Fig. 3). Due to a lower pH of water-immersed pastes, slag in such condition is much more difficult to be decomposed and thus has a lower reaction degree as shown in Fig. 4. A lower reaction degree of slag will then lead to a lower formation rate of reaction products as identified by XRD and TGA (Figs. 6 and 8). As a result, AAS pastes soaked in water have both larger gel pores and capillary pores

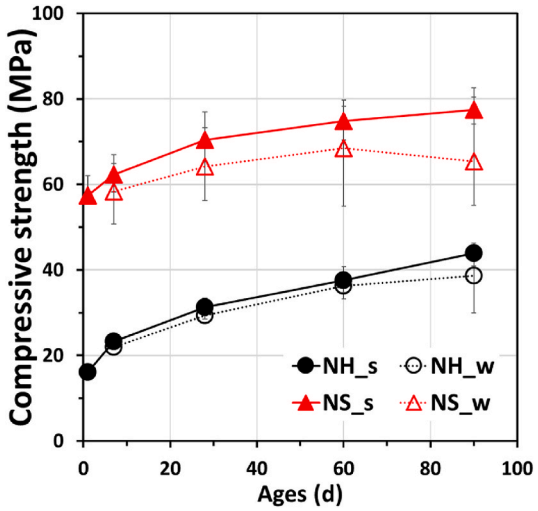


**Fig. 15.** Compressive strength of AAS pastes under sealed (s) and water immersion (w) conditions.

compared with sealed pastes (Fig. 14).

### 4.2. Gel decomposition

During long-term water immersion, the chemical property of gels is gradually changed with time. The FTIR results show that the polymerization degree of gels is increased as a function of leaching time (Fig. 9 (C) and **(D)**), which is probably attributed to the gel decalcification. Meanwhile, EDS results also collect some useful information in terms of gel decalcification and desodiumization. As shown in Fig. 12, compared with sealed AAS pastes, water-immersed pastes have lower Ca/Si and Na/Si ratios of gels and even Na ions can completely leach out after 90 day of water immersion. These results all reach a consensus that long-term water immersion will cause the change/reorganization of C–N-A-S-H gels. The constant change/reorganization of gels may further trigger the gel decomposition as the extension of immersion time. The drop in the contents of gels and hydrotalcite from 60 d to 90 d is double confirmed by XRD and TGA tests (Figs. 6 and 8). Furthermore, the increment of gel pore in NS-based water-immersed pastes from 60 d to 90 d again verify the gel decomposition (Fig. 14). These results indicate that leaching is really an issue to be concerned in long term, especially in view of gel decomposition.

### 4.3. Carbonation

As the leaching of alkali and hydroxide ions of AAS pastes, the pH of leachate is increased over 13 with time (Fig. 2). The external $CO_2$ in the air is much easier to dissolve into an alkaline solution. The soluble $CO_2$ in the leachate will hydrolyze to $CO_3^{2-}$ ion and then the $CO_3^{2-}$ ion can react with $Ca^{2+}$ ions released from AAS pastes to form the calcium carbonate (Fig. 5). Meanwhile, the layer of calcium carbonate is also detected on the surface of AAS pastes (Fig. 11). XRD and TGA results show that the content of calcium carbonate in the water-immersed AAS paste increase with time (Figs. 6 and 8). Although gel carbonation will aggravate gel decalcification and gel decomposition of an AAS paste, fortunately, calcium carbonate can be rarely found in the internal part of the paste.

In summary, this work highlights three mechanisms behind the degradation of piece AAS pastes subject to tap water immersion. Based on the understanding of these results, the insights into the behaviors of AAS subjected to water contribute to a further understanding of the durability of AAS such as freeze-thaw [75,76], chloride penetration [77], sulfate corrosion [78–80], and efflorescence [13,81–84], where external water and leaching are always involved. Even though this study used a small, representative sample, the detailed trends for each condition require further investigation. For example, employing a 1 d cured 2–4 mm piece AAS sample for the leaching test is to simulate the most severe conditions and then reveal all the potential degradation mechanisms. The moisture in water curing in practice would not move away like water immersion in this work (weekly refreshed tap water). In addition, AAS concretes in practice commonly contain a large volume of sand and gravel. These aggregates are able to largely enhance the tortuosity of the ionic migration path, and thus the concrete structure can not be thoroughly penetrated as in the case of small-scale samples, which is beneficial for mitigating the adverse effect caused by leaching. As a result, the degradation of real AAS concretes may not be as sharp as presented in this study. Further investigations are expected to focus on larger scales.

## 5. Conclusions

In this study, the degradation of AAS pastes under water-immersed condition was investigated. The mechanisms behind were revealed. Based on the results and discussion, the following conclusions can be drawn:

1. An amount of alkali and hydroxide ions in AAS pastes are liable to leach out under water-immersed condition. The drop in pH of the pore solution is identified as a function of immersion time, which subsequently hinders the dissolution of slag. A low reaction degree of slag in water-immersed paste is detrimental to the formation of reaction products and microstructure development.
2. C–N-A-S-H gels of AAS paste in water-immersed condition are gradually changed as a function of time. In terms of the FTIR results, the AAS paste after water immersion has a more cross-linked gel structure. In addition, both Ca/Si and Na/Si ratios of gels are decreased as prolong the immersion time, and Na can completely escape from gels after 90 days of immersion. Moreover, constant gel decalcification and desodiumization can lead to gel decomposition. The drop of gel content in water-immersed samples from 60 d to 90 d is detected, which indicates that C–N-A-S-H gels formed in AAS system are unstable after long-term water immersion.
3. The hydroxide ions released from AAS pastes increase the pH of the leachate, which contributes to capturing external $CO_2$. The soluble $CO_2$ will then react with Ca ions leached from AAS pastes to constantly form calcium carbonate in the leachate and on the surface of the paste. Although the content of calcium carbonate in water-

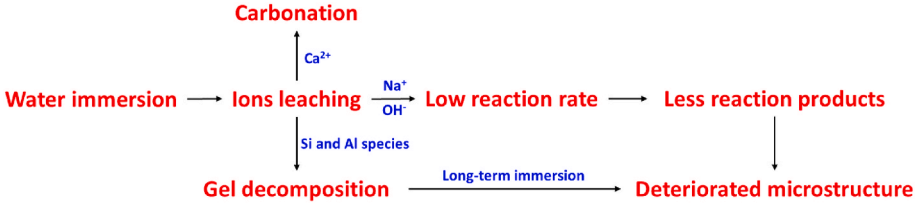


**Fig. 16.** Flowchart of degradation mechanisms of AAS pastes subject to water immersion.

immersed paste increases with time, a trace of carbonation in the internal matrix is rarely found.

4. With a low reaction degree of slag, gel decomposition and carbonation, a deteriorated pore structure of a water-immersed AAS paste is determined. Generally, the insights shown by this work indicate that water has significant impacts on the surface area of an AAS paste. Further studies in terms of leaching problems are expected to be carried out on a much bigger scale.

## CRediT authorship contribution statement

Chen Liu: Methodology, Investigation, Writing - original draft. Xuhui liang: Investigation. Chen Yun: Investigation. Zhenming Li: Conceptualization, Methodology, Supervision, Writing - review & editing. Guang Ye: Supervision, Project administration. Writing - review & editing.

## Declaration of competing interest

The authors declare that they have no known conflict of interest.

## Data availability

Data will be made available on request.

## Acknowledgment

Chen Liu, Xuhui Liang and Yun Chen would like to acknowledge the funding supported by the China Scholarship Council (CSC) under grants No. 201906950102, No. 201806050051 and No. 201906150022, respectively.

## Appendix

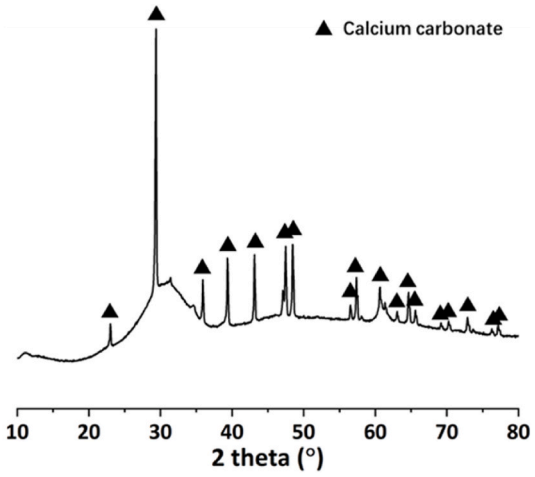


**Fig. A1.** Residue of AAS paste after SAM.

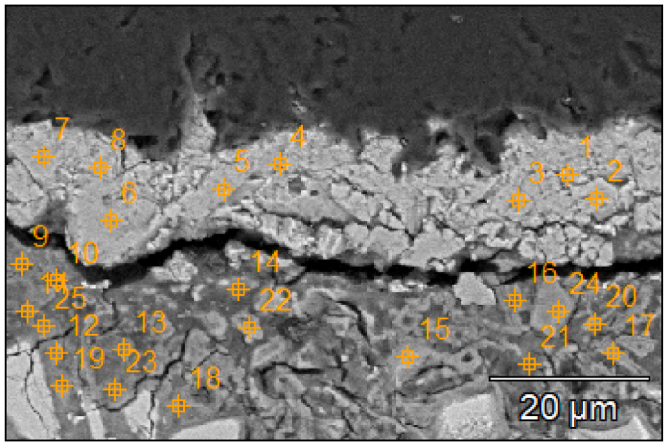


**Fig. A2.** Point analysis of the surface part of water-immersed AAS pastes

**Table A1**
Elemental composition of AAS pastes (atom %)

| | C | O | F | Na | Mg | Al | Si | S | K | Ca | Ti | Mo |
|---|---|---|---|---|---|---|---|---|---|---|---|---|
| ***pt1*** | 11.046 | 53.111 | | | 0.181 | | | | | 35.663 | | |
| ***pt2*** | 9.182 | 47.160 | | | 0.213 | | | | | 43.316 | | 0.130 |
| ***pt3*** | 11.611 | 50.807 | | | | | 0.163 | | | 37.419 | | |
| ***pt4*** | 9.778 | 50.969 | | | | | 0.266 | | | 38.987 | | |
| ***pt5*** | 10.806 | 56.080 | | | | | | | | 33.113 | | |
| ***pt6*** | 10.302 | 58.936 | | | 0.184 | | | | | 30.578 | | |
| ***pt7*** | 10.901 | 59.615 | | | 0.043 | | 0.089 | | | 29.352 | | |
| ***pt8*** | 10.922 | 58.091 | | | 0.337 | | | | | 30.649 | | |
| ***pt9*** | 12.233 | 53.816 | 1.098 | | 9.040 | 5.982 | 13.875 | 0.454 | 0.130 | 3.100 | 0.273 | |
| ***pt10*** | 15.336 | 43.664 | | | 8.721 | 6.391 | 17.201 | 0.702 | | 7.650 | 0.336 | |
| ***pt11*** | 19.093 | 49.222 | 0.085 | 0.181 | 5.705 | 5.016 | 16.035 | 0.226 | 0.152 | 4.022 | 0.264 | |
| ***pt12*** | 18.008 | 52.539 | 0.000 | | 5.824 | 4.873 | 14.191 | 0.257 | 0.140 | 3.980 | 0.188 | |
| ***pt13*** | 13.184 | 55.720 | | | 7.494 | 5.460 | 13.698 | 0.378 | 0.139 | 3.659 | 0.267 | |
| ***pt14*** | 14.536 | 41.175 | 0.517 | | 7.486 | 6.076 | 21.657 | 0.428 | 0.189 | 7.525 | 0.411 | |
| ***pt15*** | 5.396 | 54.029 | | 0.307 | 5.006 | 7.213 | 15.850 | 0.603 | 0.252 | 10.674 | 0.670 | |
| ***pt16*** | 11.582 | 49.477 | 0.000 | 0.134 | 10.410 | 7.480 | 15.880 | 0.667 | | 4.017 | 0.352 | |
| ***pt17*** | 8.631 | 48.433 | | | 10.420 | 7.601 | 17.088 | 0.765 | 0.160 | 6.395 | 0.507 | |
| ***pt18*** | 11.435 | 55.853 | 0.000 | | 4.548 | 4.577 | 17.216 | 0.212 | 0.176 | 5.715 | 0.269 | |
| ***pt19*** | 6.557 | 57.871 | | | 3.828 | 4.658 | 17.877 | 0.289 | 0.129 | 8.476 | 0.314 | |
| ***pt20*** | 21.948 | 45.299 | | | 8.482 | 6.011 | 13.814 | 0.484 | 0.153 | 3.595 | 0.213 | |
| ***pt21*** | 40.510 | 27.777 | | 0.459 | 2.175 | 3.367 | 16.570 | | 0.394 | 8.479 | 0.270 | |
| ***pt22*** | 16.249 | 59.013 | | | 8.349 | 5.027 | 8.989 | 0.401 | | 1.857 | 0.114 | |
| ***pt23*** | 16.785 | 57.120 | 0.000 | | 3.633 | 3.882 | 15.351 | | 0.222 | 2.837 | 0.168 | |
| ***pt24*** | 6.797 | 56.114 | | | 7.377 | 8.905 | 15.270 | 0.226 | | 4.444 | 0.866 | |
| ***pt25*** | 10.128 | 53.839 | 0.000 | | 10.511 | 7.777 | 12.335 | 0.720 | | 3.733 | 0.956 | |

## References


[1] J.L. Provis, Alkali-activated materials, Cement Concr. Res. 114 (2018) 40–48, https://doi.org/10.1016/j.cemconres.2017.02.009.

[2] C. Shi, A.F. Jiménez, A. Palomo, New cements for the 21st century: the pursuit of an alternative to Portland cement, Cement Concr. Res. 41 (2011) 750–763, https://doi.org/10.1016/j.cemconres.2011.03.016.

[3] J.L. Provis, A. Palomo, C. Shi, Advances in understanding alkali-activated materials, Cement Concr. Res. 78 (2015) 110–125, https://doi.org/10.1016/j.cemconres.2015.04.013.

[4] T. Bakharev, Resistance of geopolymer materials to acid attack, Cement Concr. Res. 35 (2005) 658–670, https://doi.org/10.1016/j.cemconres.2004.06.005.

[5] T. Luukkonen, Z. Abdollahnejad, J. Yliniemi, P. Kinnunen, M. Illikainen, One-part alkali-activated materials: a review, Cement Concr. Res. 103 (2018) 21–34, https://doi.org/10.1016/j.cemconres.2017.10.001.

[6] A. Fernández-Jiménez, J.Y. Pastor, A. Martín, A. Palomo, High-temperature resistance in alkali-activated cement, J. Am. Ceram. Soc. 93 (2010) 3411–3417.

[7] V.S. Athira, A. Bahurudeen, M. Saljas, K. Jayachandran, Influence of different curing methods on mechanical and durability properties of alkali activated binders, Construct. Build. Mater. 299 (2021), 123963, https://doi.org/10.1016/j.conbuildmat.2021.123963.

[8] P. Termkhajornkit, T. Nawa, K. Kurumisawa, Effect of water curing conditions on the hydration degree and compressive strengths of fly ash–cement paste, Cem. Concr. Compos. 28 (2006) 781–789, https://doi.org/10.1016/j.cemconcomp.2006.05.018.

[9] F. Sajedi, H.A. Razak, H. Bin Mahmud, P. Shafigh, Relationships between compressive strength of cement–slag mortars under air and water curing regimes, Construct. Build. Mater. 31 (2012) 188–196, https://doi.org/10.1016/j.conbuildmat.2011.12.056.

[10] S.A. Bernal, J.L. Provis, Durability of alkali-activated materials: progress and perspectives, J. Am. Ceram. Soc. 97 (2014) 997–1008, https://doi.org/10.1111/jace.12831.

[11] G. Huang, Y. Ji, L. Zhang, J. Li, Z. Hou, The influence of curing methods on the strength of MSWI bottom ash-based alkali-activated mortars: the role of leaching of OH− and free alkali, Construct. Build. Mater. 186 (2018) 978–985, https://doi.org/10.1016/j.conbuildmat.2018.07.224.

[12] C.L. Hwang, D.H. Vo, V.A. Tran, M.D. Yehualaw, Effect of high MgO content on the performance of alkali-activated fine slag under water and air curing conditions, Construct. Build. Mater. 186 (2018) 503–513, https://doi.org/10.1016/j.conbuildmat.2018.07.129.

[13] X. Yao, T. Yang, Z.Z. Zhang, Y. Wang, X. Liu, W.D. Zhang, Z. Li, Y. Zhang, Y. Li, Y. Ren, K. Sun, X. Peng, S. Wang, L. Zeng, P. Ran, G. Ji, M.A. Longhi, E. D. Rodríguez, B. Walkley, Z.Z. Zhang, A.P. Kirchheim, S.P. Kang, S.J. Kwon, X. Xue, Y.L. Liu, J.G. Dai, C.S. Poon, W.D. Zhang, P. Zhang, Z.Z. Zhang, J.L. Provis, X. Ma, A. Reid, H. Wang, J.L. Provis, A. Reid, X. Yao, T. Yang, Z.Z. Zhang, J.L. Provis, A. Reid, H. Wang, R.R. Lloyd, J.L. Provis, J.S.J. Van Deventer, Compressive strength development and shrinkage of alkali-activated fly ash–slag blends associated with efflorescence, Mater. Struct. 49 (2016) 165–177, https://doi.org/10.1016/j.cemconcomp.2018.06.010.

[14] H. El-Hassan, E. Shehab, A. Al-Sallamin, Effect of curing regime on the performance and microstructure characteristics of alkali-activated slag-fly ash blended concrete, J. Sustain. Cem. Mater. 10 (2021) 289–317, https://doi.org/10.1080/21650373.2021.1883145.

[15] H. El-Hassan, E. Shehab, A. Al-Sallamin, Influence of different curing regimes on the performance and microstructure of alkali-activated slag concrete, J. Mater. Civ. Eng. 30 (2018), 4018230.

[16] Y. Zhu, M.A. Longhi, A. Wang, D. Hou, H. Wang, Z. Zhang, Alkali leaching features of 3-year-old alkali activated fly ash-slag-silica fume: for a better understanding of stability, Compos. B Eng. 230 (2021), 109469, https://doi.org/10.1016/j.compositesb.2021.109469.

[17] S. Park, H.N. Yoon, J. Seo, H.K. Lee, J.G. Jang, Structural evolution of binder gel in alkali-activated cements exposed to electrically accelerated leaching conditions, J. Hazard Mater. 387 (2020), 121825, https://doi.org/10.1016/j.jhazmat.2019.121825.

[18] Z. Jia, R. Cao, C. Chen, Y. Zhang, Using in-situ observation to understand the leaching behavior of Portland cement and alkali-activated slag pastes, Compos. B Eng. 177 (2019), 107366, https://doi.org/10.1016/j.compositesb.2019.107366.

[19] R.S. Barneyback Jr., S. Diamond, Expression and analysis of pore fluids from hardened cement pastes and mortars, Cement Concr. Res. 11 (1981) 279–285.

[20] V. Kocaba, E. Gallucci, K.L. Scrivener, Methods for determination of degree of reaction of slag in blended cement pastes, Cement Concr. Res. 42 (2012) 511–525, https://doi.org/10.1016/j.cemconres.2011.11.010.

[21] E. Demoulian, C. Vernet, F. Hawthorn, P. Gourdin, Slag content determination in cements by selective dissolution, in: Proc. 7th Int. Congr. Chem. Cem. Paris, Fr., 1980, pp. 151–156.

[22] J.S. Lumley, R.S. Gollop, G.K. Moir, H.F.W. Taylor, Degrees of reaction of the slag in some blends with Portland cements, Cement Concr. Res. 26 (1996) 139–151.

[23] J.I. Escalante, L.Y. Gomez, K.K. Johal, G. Mendoza, H. Mancha, J. Mendez, Reactivity of blast-furnace slag in Portland cement blends hydrated under different conditions, Cement Concr. Res. 31 (2001) 1403–1409.

[24] P.E. Stutzman, Guide for X-Ray Powder Diffraction Analysis of Portland Cement and Clinker, US Department of Commerce, Technology Administration, National Institute of Standards and Technology, Office of Applied Economics, Building and Fire Research Laboratory, 1996.

[25] R. Snellings, J. Chwast, Ö. Cizer, N. De Belie, Y. Dhandapani, P. Durdzinski, J. Elsen, J. Haufe, D. Hooton, C. Patapy, M. Santhanam, K. Scrivener, D. Snoeck, L. Steger, S. Tongbo, A. Vollpracht, F. Winnefeld, B. Lothenbach, Report of TC 238-SCM: hydration stoppage methods for phase assemblage studies of blended cements—results of a round robin test, Mater. Struct. 51 (2018) 111, https://doi.org/10.1617/s11527-018-1237-5.

[26] B.S.I. NEN-EN, 196-1, Methods of Testing Cement—Part 1: Determination of Strength, BSI London, UK, 2016.

[27] C. Shi, R.L. Day, A calorimetric study of early hydration of alkali-slag cements, Cement Concr. Res. 25 (1995) 1333–1346.

[28] Z. Huanhai, W. Xuequan, X. Zhongzi, T. Mingshu, Kinetic study on hydration of alkali-activated slag, Cement Concr. Res. 23 (1993) 1253–1258, https://doi.org/10.1016/0008-8846(93)90062-E.

[29] B.S. Gebregziabiher, R. Thomas, S. Peethamparan, Very early-age reaction kinetics and microstructural development in alkali-activated slag, Cem. Concr. Compos. 55 (2015) 91–102, https://doi.org/10.1016/j.cemconcomp.2014.09.001.

[30] M. Ben Haha, G. Le Saout, F. Winnefeld, B. Lothenbach, Influence of activator type on hydration kinetics, hydrate assemblage and microstructural development of alkali activated blast-furnace slags, Cement Concr. Res. 41 (2011) 301–310, https://doi.org/10.1016/j.cemconres.2010.11.016.

[31] K.C. Newlands, M. Foss, T. Matchei, J. Skibsted, D.E. Macphee, Early stage dissolution characteristics of aluminosilicate glasses with blast furnace slag-and fly-ash-like compositions, J. Am. Ceram. Soc. 100 (2017) 1941–1955.

[32] S.-Y. Hong, F.P. Glasser, Alkali sorption by CSH and CASH gels: Part II. Role of alumina, Cement Concr. Res. 32 (2002) 1101–1111.

[33] E. L'Hôpital, B. Lothenbach, K. Scrivener, D.A. Kulik, Alkali uptake in calcium alumina silicate hydrate (CASH), Cement Concr. Res. 85 (2016) 122–136.

[34] A. Fernández-Jiménez, A. Palomo, M. Criado, Alkali activated fly ash binders. A comparative study between sodium and potassium activators, Mater. Construcción 56 (2006) 51–65.

[35] Y. Zuo, M. Nedeljković, G. Ye, Pore solution composition of alkali-activated slag/fly ash pastes, Cement Concr. Res. 115 (2019) 230–250, https://doi.org/10.1016/j.cemconres.2018.10.010.

[37] D.M. Kern, The hydration of carbon dioxide, J. Chem. Educ. 37 (1960) 14.

[38] W. Stumm, J.J. Morgan, Aquatic Chemistry: Chemical Equilibria and Rates in Natural Waters, John Wiley & Sons, 2012.

[39] C. Liu, L. Yang, Z. Li, S. Nie, C. Hu, F. Wang, Improve the long-term property of heat-cured mortars blended with fly ash by internal curing, J. Build. Eng. 54 (2022), 104624. https://doi.org/10.1016/j.jobe.2022.104624.

[40] B. Lagerblad, Carbon Dioxide Uptake during Concrete Life Cycle: State of the Art, Swedish Cement and Concrete Research Institute Stockholm, 2005.

[41] S. von Greve-Dierfeld, B. Lothenbach, A. Vollpracht, B. Wu, B. Huet, C. Andrade, C. Medina, C. Thiel, E. Gruyaert, H. Vanoutrive, I.F. Saéz del Bosque, I. Ignjatovic, J. Elsen, J.L. Provis, K. Scrivener, K.C. Thienel, K. Sideris, M. Zajac, N. Alderete, Ö. Cizer, P. Van den Heede, R.D. Hooton, S. Kamali-Bernard, S.A. Bernal, Z. Zhao, Z. Shi, N. De Belie, Understanding the carbonation of concrete with supplementary cementitious materials: a critical review by RILEM TC 281-CCC. https://doi.org/10.1617/s11527-020-01558-w, 2020.

[42] M. Nedeljković, Carbonation mechanism of alkali-activated fly ash and slag materials in view of long-term performance predictions. https://doi.org/10.4233/uuid, 2019.

[43] X. Ke, S.A. Bernal, J.L. Provis, B. Lothenbach, Thermodynamic modelling of phase evolution in alkali-activated slag cements exposed to carbon dioxide, Cement Concr. Res. 136 (2020), 106158, https://doi.org/10.1016/j.cemconres.2020.106158.

[44] S.-D. Wang, K.L. Scrivener, Hydration products of alkali activated slag cement, Cement Concr. Res. 25 (1995) 561–571, https://doi.org/10.1016/0008-8846(95)00045-E.

[45] E. Kanezaki, Thermal behavior of the hydrotalcite-like layered structure of Mg and Al-layered double hydroxides with interlayer carbonate by means of in situ powder HTXRD and DTA/TG, Solid State Ionics 106 (1998) 279–284.

[46] K. Rozov, U. Berner, C. Taviot-Gueho, F. Leroux, G. Renaudin, D. Kulik, L. W. Diamond, Synthesis and characterization of the LDH hydrotalcite–pyroaurite solid-solution series, Cement Concr. Res. 40 (2010) 1248–1254.

[47] G. Villain, M. Thiery, G. Platret, Measurement methods of carbonation profiles in concrete: thermogravimetry, chemical analysis and gammadensimetry, Cement Concr. Res. 37 (2007) 1182–1192, https://doi.org/10.1016/j.cemconres.2007.04.015.

[48] J.I. Escalante-García, A.F. Fuentes, A. Gorokhovsky, P.E. Fraire-Luna, G. Mendoza-Suarez, Hydration products and reactivity of blast-furnace slag activated by various alkalis, J. Am. Ceram. Soc. 86 (2003) 2148–2153.

[49] R. Chambers, B.W. Zweifach, Intercellular cement and capillary permeability, Physiol. Rev. 27 (1947) 436–463.

[50] W.K.W. Lee, J.S.J. Van Deventer, Use of infrared spectroscopy to study geopolymerization of heterogeneous amorphous aluminosilicates, Langmuir 19 (2003) 8726–8734.

[51] I. Garcia-Lodeiro, A. Palomo, A. Fernández-Jiménez, D.E. MacPhee, Compatibility studies between N-A-S-H and C-A-S-H gels. Study in the ternary diagram Na2O-CaO-Al2O3-SiO 2-H2O, Cement Concr. Res. 41 (2011) 923–931, https://doi.org/10.1016/j.cemconres.2011.05.006.

[52] C.A. Rees, J.L. Provis, G.C. Lukey, J.S.J. Van Deventer, The mechanism of geopolymer gel formation investigated through seeded nucleation, Colloids Surfaces A Physicochem. Eng. Asp. 318 (2008) 97–105.

[53] P. Yu, R.J. Kirkpatrick, B. Poe, P.F. McMillan, X. Cong, Structure of calcium silicate hydrate (C-S-H): near-, Mid-, and Far-infrared spectroscopy, J. Am. Ceram. Soc. 82 (1999) 742–748.

[54] E. Bernard, Y. Yan, B. Lothenbach, Effective cation exchange capacity of calcium silicate hydrates (C-S-H), Cement Concr. Res. 143 (2021), 106393, https://doi.org/10.1016/j.cemconres.2021.106393.

[55] M. Palacios, F. Puertas, Effect of carbonation on alkali-activated slag paste, J. Am. Ceram. Soc. 89 (2006) 3211–3221.

[56] R.J. Myers, S.A. Bernal, J.D. Gehman, J.S.J. Van Deventer, J.L. Provis, The role of al in cross-linking of alkali-Activated slag cements, J. Am. Ceram. Soc. 98 (2015) 996–1004, https://doi.org/10.1111/jace.13360.

[57] O. Burciaga-Díaz, J.I. Escalante-García, Structure, mechanisms of reaction, and strength of an alkali-activated blast-furnace slag, J. Am. Ceram. Soc. 96 (2013) 3939–3948, https://doi.org/10.1111/jace.12620.

[58] J.J. Chen, J.J. Thomas, H.F.W. Taylor, H.M. Jennings, Solubility and structure of calcium silicate hydrate, Cement Concr. Res. 34 (2004) 1499–1519, https://doi.org/10.1016/j.cemconres.2004.04.034.

[59] S.A. Bernal, J.L. Provis, B. Walkley, R. San Nicolas, J.D. Gehman, D.G. Brice, A. R. Kilcullen, P. Duxson, J.S.J. Van Deventer, Gel nanostructure in alkali-activated binders based on slag and fly ash, and effects of accelerated carbonation, Cement Concr. Res. 53 (2013) 127–144, https://doi.org/10.1016/j.cemconres.2013.06.007.

[60] S.A. Bernal, R. San Nicolas, J.L. Provis, R. Mejía De Gutiérrez, J.S.J. Van Deventer, Natural carbonation of aged alkali-activated slag concretes, Mater. Struct. Constr. 47 (2014) 693–707, https://doi.org/10.1617/s11527-013-0089-2.

[61] S.A. Bernal, J.L. Provis, D.G. Brice, A. Kilcullen, P. Duxson, J.S.J. Van Deventer, Accelerated carbonation testing of alkali-activated binders significantly underestimates service life: the role of pore solution chemistry, Cement Concr. Res. 42 (2012) 1317–1326, https://doi.org/10.1016/j.cemconres.2012.07.002.

[62] B. Walkley, R. San Nicolas, M.A. Sani, G.J. Rees, J.V. Hanna, J.S.J. van Deventer, J. L. Provis, Phase evolution of C-(N)-A-S-H/N-A-S-H gel blends investigated via alkali-activation of synthetic calcium aluminosilicate precursors, Cement Concr. Res. 89 (2016) 120–135, https://doi.org/10.1016/j.cemconres.2016.08.010.

[63] F. Škvára, L. Kopecký, L. Myšková, V.Í.T. Šmilauer, L. Alberovská, L. Vinšová, Aluminosilicate polymers - influence of elevated temperatures, efflorescence, Ceram. - Silikaty. 53 (2009) 276–282.

[64] H.F.W. Taylor, Cement Chemistry, Thomas Telford London, 1997.

[65] M. Ben Haha, B. Lothenbach, G. Le Saout, F. Winnefeld, Influence of slag chemistry on the hydration of alkali-activated blast-furnace slag - Part I: effect of MgO, Cement Concr. Res. 41 (2011) 955–963, https://doi.org/10.1016/j.cemconres.2011.05.002.

[66] M. Ben Haha, B. Lothenbach, G. Le Saout, F. Winnefeld, Influence of slag chemistry on the hydration of alkali-activated blast-furnace slag - Part II: effect of Al2O3, Cement Concr. Res. 42 (2012) 74–83, https://doi.org/10.1016/j.cemconres.2011.08.005.

[67] I.G. Richardson, Tobermorite/jennite-and tobermorite/calcium hydroxide-based models for the structure of CSH: applicability to hardened pastes of tricalcium silicate, β-dicalcium silicate, Portland cement, and blends of Portland cement with blast-furnace slag, metakaolin, Cem, Concr. Res. 34 (2004) 1733–1777.

[68] S.-D. Wang, K.L. Scrivener, 29Si and 27Al NMR study of alkali-activated slag, Cement Concr. Res. 33 (2003) 769–774.

[69] A.C.A. Muller, Characterization of Porosity & CSH in Cement Pastes by $^{1}$H NMR, EPFL, 2014.

[70] M.H. Hubler, J.J. Thomas, H.M. Jennings, Influence of nucleation seeding on the hydration kinetics and compressive strength of alkali activated slag paste, Cement Concr. Res. 41 (2011) 842–846, https://doi.org/10.1016/j.cemconres.2011.04.002.

[71] Z. Li, T. Lu, Y. Chen, B. Wu, G. Ye, Prediction of the autogenous shrinkage and microcracking of alkali-activated slag and fly ash concrete, Cem. Concr. Compos. 117 (2021), 103913, https://doi.org/10.1016/j.cemconcomp.2020.103913.

[72] H. Ye, C. Cartwright, F. Rajabipour, A. Radlińska, Understanding the drying shrinkage performance of alkali-activated slag mortars, Cem. Concr. Compos. 76 (2017) 13–24.

[73] Z. Li, T. Lu, X. Liang, H. Dong, G. Ye, Mechanisms of autogenous shrinkage of alkali-activated slag and fly ash pastes, Cement Concr. Res. 135 (2020), 106107, https://doi.org/10.1016/j.cemconres.2020.106107.

[74] Z. Li, M. Wyrzykowski, H. Dong, J. Granja, M. Azenha, P. Lura, Internal curing by superabsorbent polymers in alkali-activated slag, Cement Concr. Res. 135 (2020), 106123, https://doi.org/10.1016/j.cemconres.2020.106123.

[75] F. Winnefeld, G.J.G. Gluth, S.A. Bernal, M.C. Bignozzi, L. Carabba, S. Chithiraputhiran, A. Dehghan, S. Dolenec, K. Dombrowski-Daube, A. Dubey, V. Ducman, Y. Jin, K. Peterson, D. Stephan, J.L. Provis, RILEM TC 247-DTA round robin test: sulfate resistance, alkali-silica reaction and freeze–thaw resistance of alkali-activated concretes, Mater. Struct. 53 (2020) 140, https://doi.org/10.1617/s11527-020-01562-0.

[76] Y. Fu, L. Cai, W. Yonggen, Freeze–thaw cycle test and damage mechanics models of alkali-activated slag concrete, Construct. Build. Mater. 25 (2011) 3144–3148.

[77] D.M. Roy, W. Jiang, M.R. Silsbee, Chloride diffusion in ordinary, blended, and alkali-activated cement pastes and its relation to other properties, Cem, Concr. Res. 30 (2000) 1879–1884.

[78] T. Bakharev, J.G. Sanjayan, Y.-B. Cheng, Sulfate attack on alkali-activated slag concrete, Cement Concr. Res. 32 (2002) 211–216.

[79] D. Coefficient, Simple Model for Alkali Leaching from Geopolymers : Effects of Raw Materials and Acetic Acid Concentration on Apparent, 2021.

[80] C. Grengg, G.J.G. Gluth, F. Mittermayr, N. Ukrainczyk, M. Bertmer, A.G. Buzanich, M. Radtke, A. Leis, M. Dietzel, Deterioration mechanism of alkali-activated materials in sulfuric acid and the influence of Cu: a micro-to-nano structural,

elemental and stable isotopic multi-proxy study, Cement Concr. Res. 142 (2021), 106373.
[81] M.A. Longhi, Z. Zhang, B. Walkley, E.D. Rodríguez, A.P. Kirchheim, Strategies for control and mitigation of efflorescence in metakaolin-based geopolymers, Cement Concr. Res. 144 (2021), https://doi.org/10.1016/j.cemconres.2021.106431.
[82] Z. Zhang, J.L. Provis, A. Reid, H. Wang, Fly ash-based geopolymers: the relationship between composition, pore structure and efflorescence, Cement Concr. Res. 64 (2014) 30–41, https://doi.org/10.1016/j.cemconres.2014.06.004.
[83] Z. Zhang, J.L. Provis, X. Ma, A. Reid, H. Wang, Efflorescence and subflorescence induced microstructural and mechanical evolution in fly ash-based geopolymers, Cem. Concr. Compos. 92 (2018) 165–177, https://doi.org/10.1016/j.cemconcomp.2018.06.010.
[84] D. Tang, C. Yang, X. Li, X. Zhu, K. Yang, L. Yu, Mitigation of efflorescence of alkali-activated slag mortars by incorporating calcium hydroxide, Construct. Build. Mater. 298 (2021), 123873, https://doi.org/10.1016/j.conbuildmat.2021.123873.